Chiang Mai J. Sci. 2024; 51(3): e2024034
https://doi.org/10.12982/CMJS.2024.034
Journal homepage : http://epg.science.cmu.ac.th/ejournal/

Research Article

Exploring the Sound Absorption and Sound Insulation Capabilities of Natural Fiber Composites: Nipa Palm Peduncle Fiber

Purintorn Chanlert [a]*, Polphat Ruamcharoen [a] and Thanate Kerdkaew [b]

[a] Faculty of Science and Technology, Songkhla Rajabhat University, Songkhla 90000 Thailand

[b] Chemistry and Biology Unit, Institute for the Promotion of Teaching Science and Technology, Bangkok 10110, Thailand

*Author for correspondence; e-mail: purintorn.ch@skru.ac.th

Received: 31 October 2023
Revised: 19 March 2024
Accepted: 20 March 2024

Abstract

This study investigates the acoustic properties of nipa palm peduncle fiber (NPPF) composites, a promising natural fiber with a tensile strength of 277 MPa, a yield strength of 49.0 MPa, and a Young's modulus of 12.0 GPa. We focus on understanding how NPPF's physical characteristics influence its sound absorption and insulation capabilities. Through experimental analysis, we found that the sample density directly affects the sound absorption coefficient (SAC) and transmission loss (TL), with denser samples exhibiting better noise reduction. Using the Johnson-Champoux-Allard-Lafarge (JCAL) model, we correlated these acoustic properties with the material's non-acoustic parameters including flow resistivity (σ), open porosity (ϕ), tortuosity (α_∞), viscous (Λ) and thermal (Λ') characteristic lengths along with static thermal permeability (k_0'). The results validate the JCAL model's predictions, offering insights into designing effective, eco-friendly acoustic materials. This study not only highlights NPPF composites' notable acoustic performance but also underlines their potential for contributing to sustainable development.

Keywords: natural fiber, Nipa palm, sound absorption coefficient, sound transmission loss, Johnson-Champoux-Allard-Lafarge (JCAL) model

1. Introduction

Noise pollution, an escalating urban concern, adversely impacts human health and necessitates urgent, sustainable mitigation strategies. Current synthetic sound absorbers, such as fiberglass [1], rock wool [2,3], and petrochemical foam [4], though effective, are ecologically unfriendly and non-renewable [3]. The exploration of natural materials alternatively presents an environmental responsibility. These bio-based solutions, derived from agricultural waste fibers or granular substances, are not only eco-friendly but also economically viable due to their abundant availability and biodegradability. Moreover, they exhibit commendable noise reduction capabilities, as recently demonstrated by studies on fibers obtained from bamboo [5], sugarcane bagasse [6], jute and luffa [7,8], and other plant fibers. Similarly, granular materials such as rice hull [9], cork [10] and rice bran [11], have demonstrated potential sound-absorbing capabilities. The physical properties of the resulting acoustic panel are significantly influenced by the type and quantities of adhesive employed to bind the natural fibers or grains. For example, panels constructed with polymer binders like resin [12] exhibit distinct physical characteristics compared to those made with cementitious materials [13]. The acoustic properties of fibrous or granular materials including shape [14], size [15] and fiber orientation [16], contribute to their acoustic performance when utilized in acoustic panel fabrication.

In this context, the nipa palm (*Nypa fruticans* Wurmb), prevalent in South and Southeast Asian mangroves [17] emerges as a promising resource. Its population density has been found to be remarkably high, reaching up to 6,400 individuals per hectare in Carey Island, Malaysia [18]. Due to its widely recognition in local community, the nipa palm is utilized to produce a variety of goods, including roofing material (thatch), cigarette paper from its leaves and various products from its sap, such as molasses, vinegar, syrup, and granulated sugar [19]. The estimated maximum daily sales per household of molasses, thatch, and syrup from the nipa palm in Pak Phanang, Nakorn Sri Thammarat province, Thailand, are 90-130 USD, 133.3 USD, and 200 USD respectively [19]. As a result, the nipa palm receives significant attention in terms of its economic value. Apart from its common application, the nipa palm is more widely used in a variety of sectors, particularly for its fiber. The remaining seed material can be used as a raw material for biomass fuel pellet production [20]. The fruit fiber can be utilized to create particleboards [21], while the fiber from the leaves and stalks can be used to create paper [22]. Nipa palm's extensive utility is attributed to its significant fiber content, which comprises cellulose, hemicellulose, and lignin [23]. Despite its high tensile strength [24] and substantial economic contributions in local communities, a few researches have been done on the usage of nipa palm fiber as composite materials in products like natural sound absorbers.

This study pioneers the investigation into nipa palm peduncle fiber (NPPF) as a novel natural porous fibrous sound absorber. The study explores the sound absorption and insulation characteristics of NPPF-based, employing rigorous experimental and computational methodologies to discern the mechanisms influencing their acoustic properties. The acoustic characteristics are correlated with Johnson-Champoux-Allard-Lafarge (JCAL) model [25–28], offering insights into the material's potential as a sustainable acoustic solution. The consequent sections detail the procedural nuances of NPPF sample preparation, acoustic evaluations, and an in-depth discussion of the findings, concluding with the implications of employing NPPF in addressing noise pollution sustainably.

2. MATERIALS AND METHOD

2.1 Sample Preparation

The preparation of cylindrical nipa palm peduncle fiber (NPPF) samples, as detailed in this study and illustrated in Figure 1, commenced with step 1, the sourcing of fresh male flower peduncles from a local mangrove in Pak Phanang district, Nakhon Si Thammarat, Thailand. Subsequently, in step 2, these peduncles were mechanically fragmented into strands with an average diameter of 0.4 mm. In step 3, the strands prepared for use were roughly 30 mm in length. To ensure the removal of moisture, step 4 involved heating the strands in a hot-air oven at 90 °C until the NPPF weight stabilized, indicating that effective moisture evaporation had occurred after heating for 1 hour. For the composite formulation, step 5, fiber content ranging from 1 to 5 g per set volume was mixed with a 10% polyvinyl alcohol (PVA) solution used as the binder, resulting in composites designated as NP-1R to NP-5R. This mixture was then homogenized and cast into a cylindrical mold (28.6 mm diameter, 40.0 mm thickness), as described in step 6, with the fiber orientation kept random. The curing process, step 7, involved keeping the samples under pressure in the mold for 24 hours and post-curing at 90°C for 90 minutes. Finally, step 8 concluded the process, with the samples being stored in a desiccator for 24 hours before testing, displaying a uniform brown color that matched the natural color of NPPF, attributed to the transparent PVA adhesive used.

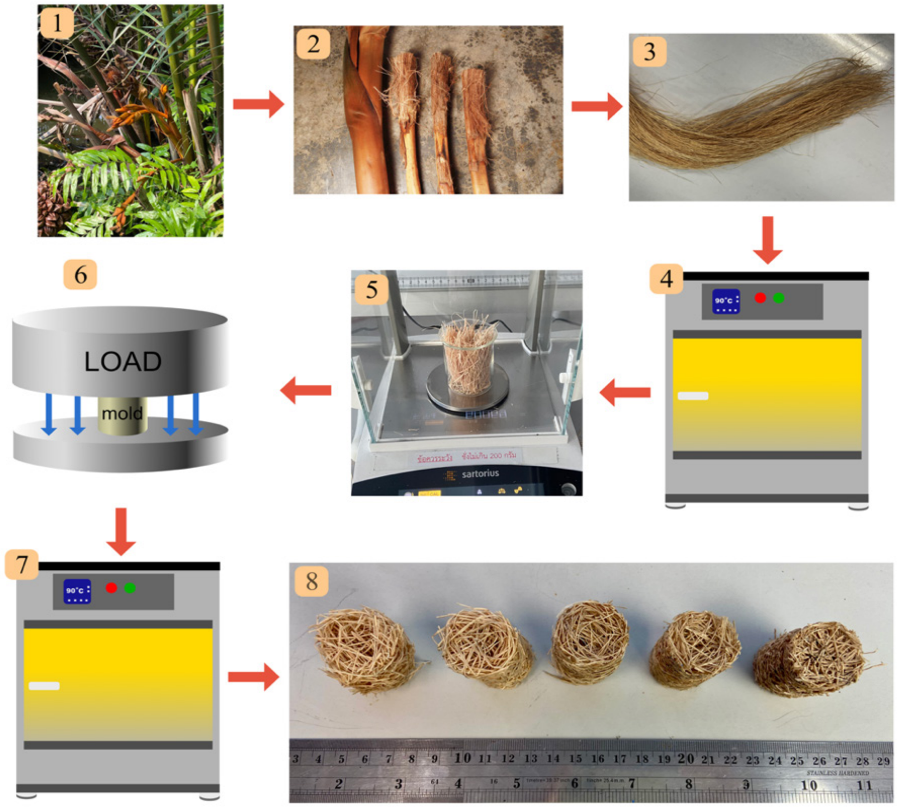

Figure 1. The preparation procedure of the porous fibrous samples made from NPPF.

2.2 Test of Fiber Mechanical Properties

Tensile strength, yield strength and Young's modulus were assessed using a universal testing machine (NRI-TS500-30B, Narin Instrument, Thailand) at a 3 mm/min crosshead speed. Five specimens of single NPPF strand were tested and the average of the values was taken.

2.3 Static Flow Resistivity Measurement

Flow resistivity (σ) is one of the most important non-acoustical parameters that explain the sound-absorbing properties of porous materials. It is a measure of the resistance of a material to the flow of air through its pores. In general, materials having a higher flow resistivity have greater sound absorption coefficients, as they are more resistant to the flow of air and, hence, more effective at absorbing sound energy. In this study, flow resistivity was examined using the procedure according to ISO-9053 [29], using the formula:

$$\sigma = (A/Qd)\Delta P \tag{1}$$

where A is the cross-sectional area, d the sample thickness, and ΔP the pressure differential across the specimen. The findings are in Table 1, with detailed correlations with SAC and TL explored in subsequent sections.

2.4 SAC and TL Measurements

The normal-incident sound absorption coefficient (SAC) was measured using an in-house two-microphone impedance tube [30,31]. It was constructed in accordance with ASTM E1050 [32] and ISO 10534 [33] standard. The diameter of the tube was precisely 28.6 mm. Its length was

Table 1. Sample density, noise reduction coefficient (NRC), 1/4-wavelength resonance frequency, non-acoustic parameters obtained from the direct measurement (σ) and least-square fitting (ϕ, α_∞, Λ, Λ', and k_0') of the JCAL model with experimental results.

Sample	Density (kg/m^3)	NRC	f_r (Hz)	σ (Pa·s·m^{-2})	ϕ	α_∞	Λ (μm)	Λ' (μm)	k_0' 10^{-9} m^2)
NP-1R	85	0.27	3735	303	0.926	1.311	353.8	400.1	20.4
NP-2R	127	0.37	3400	956	0.888	1.290	187.5	388.5	13.6
NP-3R	174	0.44	2672	2309	0.849	1.516	143.9	143.9	7.79
NP-4R	212	0.51	2419	5022	0.674	1.457	86.1	155.0	6.20
NP-5R	239	0.54	2246	9356	0.650	1.638	71.7	100.3	3.43

1,000 mm which was sufficient for sound wave to become normal incident when reaching the sample surface. Sound signals were captured by laboratory-grade microphones (GRAS 40PP; GRAS Sound & Vibration, Skovlytoften, Denmark). The signals were collected to the computer using a data acquisition device (NI-9230; National Instruments, Austin, TX, USA). Data collection and interpretation were performed using data acquisition module in PYTHON. Non-acoustic parameters, as prescribed by the JCAL model, will be deduced through the optimization of computed SAC spectra against experimental data. To enhance the fidelity of the fitting process, multiple SAC spectra were acquired under varying conditions, specifically with air gap distances of 0 mm, 20 mm, and 40 mm between the specimen and the backing plate.

Concurrently, the transmission loss (TL) at normal incidence was quantified utilizing an in-house four-microphone impedance tube [30] conforming to the ASTM-E2611 standard [34].

3. Results and discussion

3.1 Fiber Characteristics

Nipa palm peduncle fibers (NPPF) display an average diameter of roughly 450 μm, as evidenced by cross-sectional image taken with a FEG-SEM (Phenom Pharos G2; Thermo Fisher Scientific, Waltham, MA, USA) as shown in Figure 2. SEM image in Figure 2 highlights the central large vessels in the peduncle and the dense fiber cells with thick walls in the outer layer, emphasizing the peduncle's role in structural support. The fibers in the frond, rich in cellulose, hemicellulose, and lignin, contribute significantly to plant cell strength [35], a characteristic given the peduncle's support function for flowers and fruits.

3.2 Fiber Mechanical Property Results

Tensile behavior of nipa palm peduncle fiber is presented in Figure 3. The stress-strain relationship for this fiber initially demonstrates a linear behavior, indicative of elastic deformation, with a Young's modulus of 12.0 GPa derived from this region. This continues until the yield point, indicating the onset of plastic deformation. The yield strength, approximated at 49.0 MPa, is identified using the 0.2% offset method, highlighted by the pink dot in Figure 3. Testing proceeds until the fiber reaches its fracture point, at which the tensile strength is determined to be approximately

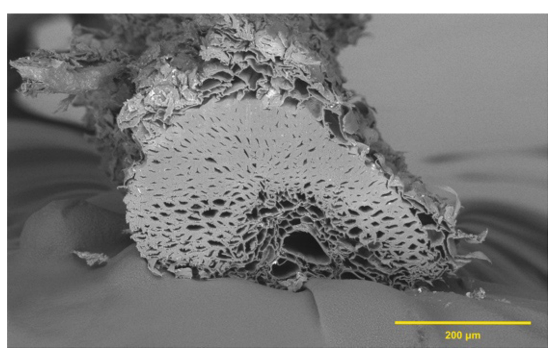

Figure 2. FEG-SEM image showing cross-sectional area of nipa palm fiber.

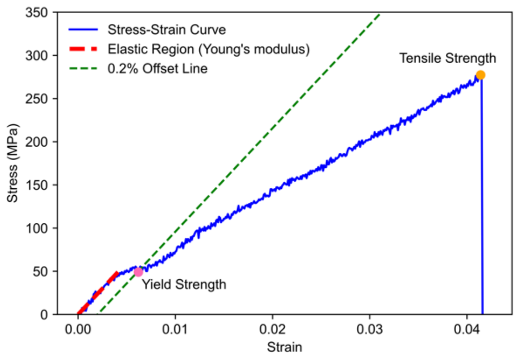

Figure 3. Stress - strain relation of a single strain of NPPF.

277 MPa, denoted by the orange dot in Figure 3. Based on these results, the fibers can be classified as high-performance natural fibers [36]. This value is comparable to that of polypropylene fibers, which presents tensile strength ranging from 50 - 600 MPa and tensile moduli in the range of 0.5 - 3.0 GPa [37].

The tensile strength of natural fibers is largely determined by their cellulose content. In a recent study by Hasan et al. [24], the tensile strength of nipa palm frond fiber with 35.1% cellulose content was found to be approximately 200 MPa, which is slightly lower to that of the peduncle strand observed in this study. This implies that the peduncle strand might also have equivalent or even higher cellulose content than the frond. Anyway, further investigation into the chemical constituents of nipa palm peduncle is necessary to verify this assumption.

3.3 Static Flow Resistivity Results

This research reveals that static flow resistivity of the porous fibrous samples, essential for interpreting sound absorption in porous materials, ranges approximately 300 to 9500 Pa·s·m^{-2} and positively correlates with sample density as shown in Table 1.

3.4 SAC and TL Results

Figure 4 (a) showcases the sound absorption coefficient (SAC) spectra, ranging from 100 to 5000 Hz. Higher SAC values signify superior sound absorption. Notably, the densest NPPF sample (NP-5R) demonstrates the peak SAC spectrum, whereas the least dense (NP-1R) records the lowest. The noise reduction coefficient (NRC) offers a simplified average of SACs at specific frequencies (250, 500, 1000, and 2000 Hz). Table 1 depicts a direct NRC and sample correlation, with NP-1R and NP-5R at the extremities. Comparatively, NP-5R's density aligns with that of analogous porous materials like palmyra palm fiber [30].

All SAC spectra display a peak-valley pattern resulting from 1/4-wavelength resonance of the frame due to longitudinal waves in the direction normal to the surface as explained by Bardot et al. [38]. Resonance frequency (f_r) can be determined by analyzing acoustic impedance spectra as shown in Figure 4 (b). Acoustic impedance comprises a real part (acoustic resistance) with a hump-like characteristic and an imaginary part (acoustic reactance). The peak in the real part indicates the resonance frequency (f_r) where surface

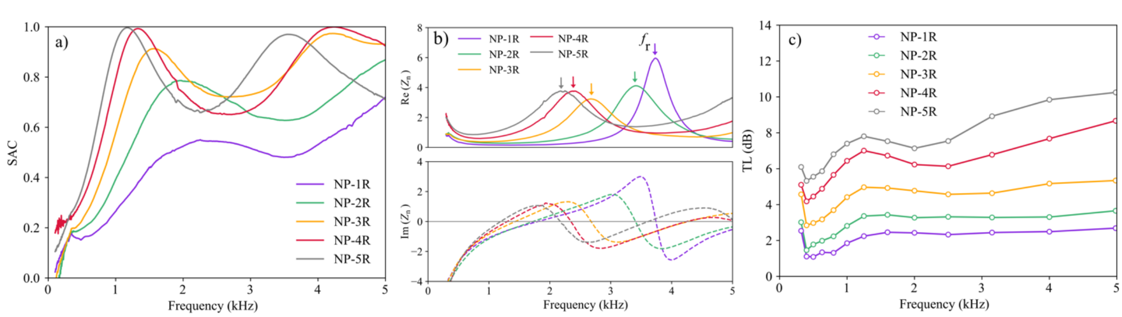

Figure 4. Normal incident SAC a), acoustic impedance b) and TL spectra of NPPF samples c).

resistance is highest. The transition from positive to negative reactance also occurs at f_r. Bardot et al. (1996) [38] describe that f_r for a rigid frame is directly proportional to bulk and shear modulus but inversely proportional to density and material thickness. In Figure 4 (b), f_r, marked by the arrow, inversely correlates with sample density. The f_r values are listed in Table 1. Figure 4 (a) demonstrates that the SAC spectrum is lowest at f_r, indicating weaker sound absorption around this frequency compared to its surroundings.

The transmission loss (TL) data, detailed in Figure 4 (c), also correlate directly with density, mirroring SAC findings. Prior studies on palmyra palm fruit fiber composites indicate TL dependency on sample density for absorbers of equal thickness [30]. samples with high density, including NPPF composites, consistently demonstrate elevated TL, affirming the anticipated outcome: NP-5R, the densest sample, exhibits the highest TL.

3.5 Johnson-Champoux-Allard-Lafarge (JCAL) Model

The Johnson-Champoux-Allard-Lafarge (JCAL) model [25–28] comprehensively portrays fluid behavior in porous materials with a rigid frame. It highlights that the sound absorption coefficient (SAC) relies on critical parameters: flow resistivity (σ), open porosity (ϕ), tortuosity (α_∞), and characteristic lengths for viscous (Λ) and thermal (Λ') aspects, along with static thermal permeability (k'_0). This model elucidates the energy dissipation of sound waves due to viscous and thermal losses, reflected in the equations for equivalent dynamic density (ρ_{eq}) and bulk modulus (K_{eq}):

$$\rho_{\mathrm{eq}}(\omega) = \frac{\alpha_\infty \rho_0}{\phi}\left[1 + \frac{\sigma\phi}{i\omega\rho_0\alpha_\infty}\left(1 + i\frac{4\alpha_\infty^2\eta\omega\rho_0}{(\sigma\Lambda\phi)^2}\right)^{1/2}\right] \tag{2}$$

$$K_{\mathrm{eq}}(\omega) = \frac{\gamma P_0}{\phi}\left(\gamma - (\gamma-1)\left[1 - i\frac{\phi\kappa}{\omega\rho_0 k'_0 C_P}\left(1 + i\frac{4k_0'^2 C_P\omega\rho_0}{\kappa(\Lambda'\phi)^2}\right)^{1/2}\right]^{-1}\right)^{-1} \tag{3}$$

where C_P is the specific heat of air at constant pressure, ρ_0 is the density of the air, ω is the sound wave's angular frequency, γ is the specific heat ratio of the air, P_0 is the atmospheric pressure, and κ is the thermal conductivity of the air. The characteristic impedance (Z_c) and the complex wave number (k_c) and can be calculated using:

$$Z_c = \sqrt{\rho_{\mathrm{eq}} K_{\mathrm{eq}}} \tag{4}$$

$$k_c = \omega\sqrt{\rho_{\mathrm{eq}}/K_{\mathrm{eq}}} \tag{5}$$

The transfer matrix method is a mathematical technique used to analyze the transmission of waves through materials. This method separates the materials into thin layers, with its inherent unique acoustic properties. The transfer matrix (T) can be expressed as follows [11,39]:

$$T = \begin{bmatrix} \cos(kd) & i(Z\sin(kd)) \\ i\sin(kd)/Z & \cos(kd) \end{bmatrix} \tag{6}$$

where d is the thickness of sample or air gap. k and Z represent k_c and Z_c for the porous absorber, and k_0 (complex wave number of the air) and Z_0 (impedance of the air) for the air gap, respectively. The total transfer matrix for the two-layer system can be obtained by multiplying the transfer matrices of each layer, as follows [11]:

$$T_{\mathrm{all}} = \prod_{i=1}^{2} T_{\mathrm{i}} = T_{\mathrm{porous}} \cdot T_{\mathrm{airgap}} = \begin{bmatrix} T_{11} & T_{12} \\ T_{21} & T_{22} \end{bmatrix} \tag{7}$$

Eventually, the surface impedance (Z_s) of the entire porous absorber-air gap system can be expressed as follows:

$$Z_s = T_{11}/T_{21} \tag{8}$$

$$\mathrm{SAC} = 1 - \left|\frac{Z_s - \rho_0 c_0}{Z_s + \rho_0 c_0}\right|^2 \tag{9}$$

The expression given in Eq.9 will serve as the mathematical model for least-squares fitting of SAC spectra of samples at simultaneously zero, 20, and 40 mm air gaps. Figure 5 depicts the comparison between experimental results (red solid line) and mathematical calculation (grey dashed line) using JCAL model with optimized non-acoustic parameters. During the least-square fitting procedure, the parameter remained fixed at values acquired through direct measurement. Conversely, the remaining parameters (ϕ, α_∞, Λ, Λ', and k'_0) underwent optimization through least-square fitting, involving a comparison between the model and experimental spectra.

Table 1 presents the observed trends in σ and α_∞ with respect to sample density. σ characterizes a material's capacity to impede static fluid flow through its porous structure. On the other hand, α_∞ quantifies the degree of pore twisting or curvature within the material, with a minimum value of 1 indicating a lack of curvature [26]. As depicted in Figure 6(a) and (c), it is evident that samples with higher densities exhibit elevated values for both σ and α_∞.

ϕ, Λ, Λ', and k'_0 exhibit an inverse relationship with sample density, as depicted in Figure 6(b), (d), and (e). In most cases, the optimized ϕ demonstrates a linear decrease, while higher-density samples, such as NP-4R and NP-5R, display a pronounced reduction in ϕ. Given that Λ' and Λ respectively represent pore size and pore interconnection dimensions [27], it is anticipated that these parameters would be smaller in high-density samples. Notably, the values of Λ' and Λ fall within a similar order of magnitude, indicating minimal disparities in pore and pore interconnection sizes. Similarly, k'_0 , which characterizes thermal exchange between the frame and fluid, particularly at low frequencies [28], is observed to be lower in samples with higher densities, consistent with the trends in the other parameters.

The density of a porous absorber has a significant effect on its TL. A higher density leads to better sound insulation properties (higher TL). The JCAL model outlines six non-acoustical parameters that have notable influence on the acoustical characteristics of porous materials, encompassing sound absorption and sound insulation [7,30].

The transmission loss (TL) at normal incidence of the porous materials can be predicted from the transfer matrix [16,30], given by:

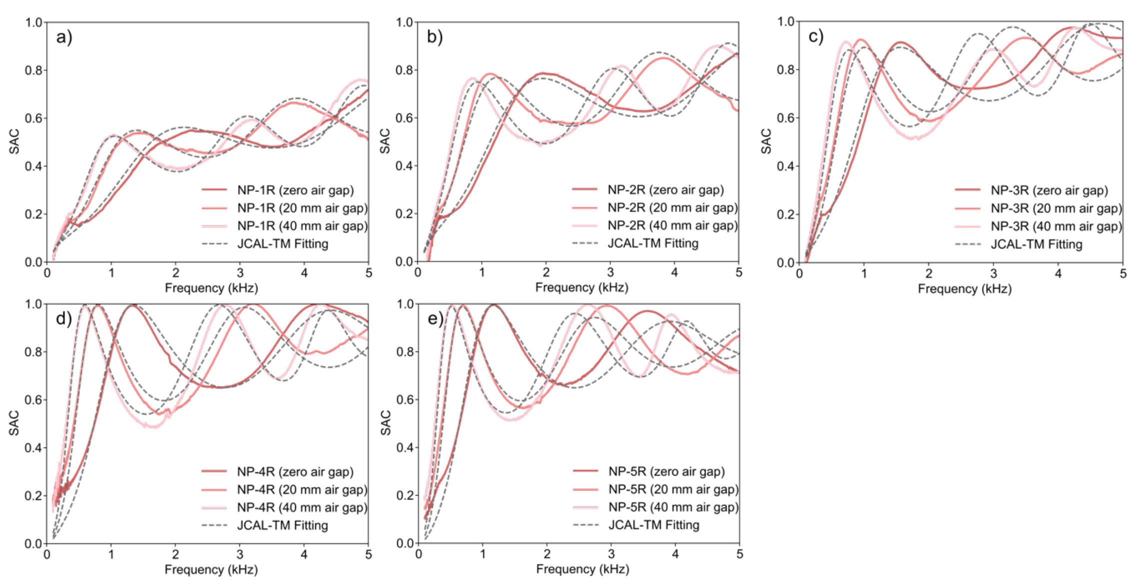

Figure 5. SAC spectra with zero, 20, and 40 mm air gaps with curves acquired from the least-square fitting using JCAL model for NP-1R a), NP-2R b), NP-3R c), NP-4R d), and NP-5R e).

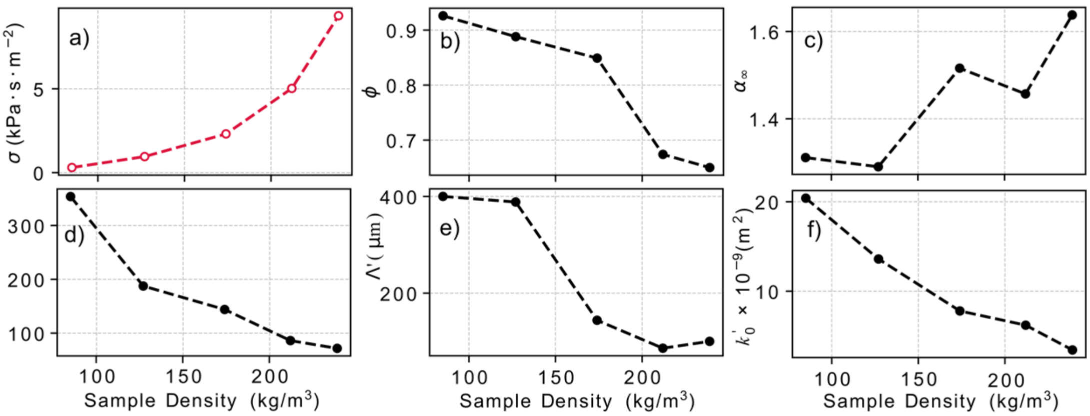

Figure 6. Six non-acoustic JCAL parameters including flow resistivity (σ) a), opened porosity b), tortuosity (α_∞) c), viscous characteristic length (Λ) d), thermal characteristic length (Λ') e), and thermal permeability (k'_0) f) .

$$\mathrm{TL} = 20\log_{10}\left|\cos(k_c d) + \frac{i}{2}\left(\frac{Z_c}{\rho_0 c_0} + \frac{\rho_0 c_0}{Z_c}\right)\sin(k_c d)\right| \tag{10}$$

From Figure 7, the calculated TL spectrum (blue dashed line) of each sample exhibit commendable agreement with the corresponding experimental data points (blue open circle). However, most results showed discrepancies of approximately 2 dB within the hump region (1,000 - 3,000 Hz), where the majority of experimental TL spectra surpass the calculated counterparts. In this study, error analysis was performed to compare the experimental results with theoretical predictions for both the sound absorption coefficient (SAC) and transmission loss (TL) at octave band frequencies. The analysis focused on two distinct frequency ranges [40]: low frequency (100-1600 Hz) and high frequency (2000-5000 Hz). The errors were calculated using the formula:

$$\mathrm{Error} = \frac{|\,exp - cal\,|}{exp} \times 100 \tag{11}$$

where *exp* and *cal* represent experimental values and the theoretical calculation of SAC and TL from JCAL model, respectively. For the low frequency range, SAC errors for NP-1R, NP-2R, NP-3R, NP-4R, and NP-5R were 20.0%, 13.5%, 19.5%, 30.2%, and 26.7%, respectively. TL errors in the same range were notably higher, at 51.5%, 45.2%, 47.6%, 29.9%, and 21.5%, respectively. In contrast, at high frequencies, SAC errors decreased across all samples to 4.0%, 3.1%, 4.3%, 3.7%, and 6.4%, respectively, with TL errors similarly reduced to 25.5%, 12.0%, 11.5%, 6.0%, and 3.6%, respectively. This patterns of SAC and TL indicate a closer alignment between experimental results and theoretical predictions at higher frequencies, highlighting the influence of frequency and material composition on the acoustic properties of NPPF composites. It is noteworthy that the NP-5R sample, characterized by the highest density, notably manifests the smallest divergence between experimental and calculated TL values.

The present investigation underscores the remarkable sound absorption capabilities of nipa palm peduncle fiber (NPPF), underscoring its substantial potential in acoustic applications. Nonetheless, achieving enhanced sound insulation properties necessitates the utilization of higher-density NPPF samples. Importantly, NPPF's environmental advantages as a natural fiber further bolster its attractiveness. The sustainable practices associated with nipa palm cultivation and harvesting guarantee minimal environmental impact and resource depletion. With a tensile strength of

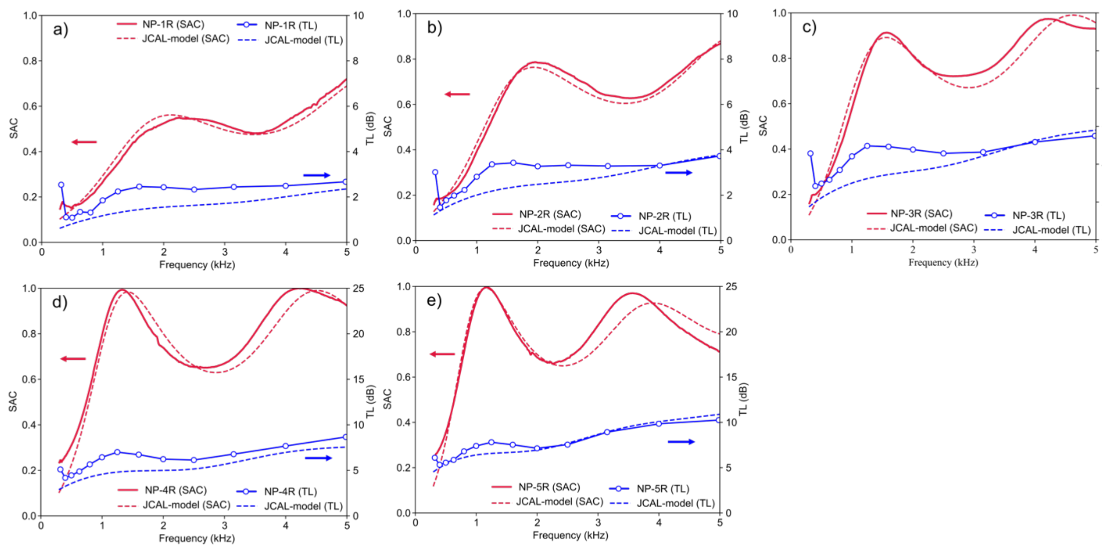

Figure 7. SAC spectra with zero, 20, and 40 mm air gaps with curves acquired from the least-square fitting using JCAL model for NP-1R a), NP-2R b), NP-3R c), NP-4R d), and NP-5R e).

270 MPa, this fiber exhibits considerable promise for the development of robust sound absorption panels. Considering these attributes, NPPF emerges as a promising eco-friendly alternative.

4. Conclusions

This study presented a comprehensive investigation into the sound absorption and sound insulation characteristics of natural fiber composites derived from nipa palm peduncle fiber (NPPF).

1. NPPF is a high-performance natural fiber, performing impressive tensile strength with approximately 277 MPa, yield strength of 49.0 MPa and a Young's modulus of 12.0 GPa.

2. The acoustic assessment resulted reveal a direct correlation between sample density and the SAC and TL of NPPF absorbers. The composites with highest density (239 kg/m^3) exhibit the highest NRC, reaching 0.54.

3. The JCAL model had been employed to explain the acoustic behaviors exhibited by this porous fibrous absorber. Fitting results demonstrated that flow resistivity and tortuosity exhibit an increasing trend with density, whereas opened porosity, viscous/thermal characteristic length, and static thermal permeability displayed an inverse relationship with density. These findings held substantial implications for the rational design and optimization of prospective sound absorbers utilizing natural fibers.

4. Future studies may extend the model's scope by incorporating an expanded range of sample thicknesses, diverse adhesive types, and a broader spectrum of sample densities. Additionally, exploring the potential of other components of the nipa palm plant presents opportunities for the development of sustainable and highly efficient acoustic materials.

Acknowledgments

The authors are thankful for the equipment support from the Faculty of Science and Technology, Songkhla Rajabhat University, Thailand.

Conflict of Interest Statement

The authors affirm that they do not have any conflicting financial interests or personal affiliations that might have impacted the research presented in this study.

References

[1] Aso S. and Kinoshita R., *J. Text. Mach. Sco. Jpn.*, 1965; **18(11)**: T649–T653. DOI 10.4188/transjtmsj1965b.18.t649.

[2] Uris A., Llopis A. and Llinares J., *Appl. Acoust.,* 1999; **58(3)**: 327–331. DOI 10.1016/S0003-682X(98)00065-6.

[3] Itewi M., *Am. J. Environ. Sci.*, 2011; **7(2)**: 161–165. DOI 10.3844/ajessp.2011.161.165.

[4] Lei L., Dauchez N. and Chazot J.D., *Appl. Acoust.,* 2018; **139**: 44–56. DOI 10.1016/j.apacoust.2018.04.010.

[5] Koizumi T., Tsujiuchi N. and Adachi A., *J. INCE Jpn.*, 2002; **4**: 157–166. DOI 10.11372/souonseigyo1977.27.210.

[6] Mehrzad S., Taban E., Soltani P., Samaei S.E. and Khavanin A., *Build. Environ.*, 2022; **211**: DOI 10.1016/j.buildenv.2022.108753.

[7] Koruk H., Ozcan A.C., Genc G. and Sanliturk K.Y., *J. Nat. Fibers.*, 2022; **19(13)**: 6239–6254. DOI 10.1080/15440478.2021.1907832.

[8] Raj M., Fatima S. and Tandon N., *Appl. Acoust.,* 2020; **159**: 107070. DOI 10.1016/j.apacoust.2019.107070.

[9] Kang C.W., Oh S.W., Lee T.B., Kang W., Matsumura J., *J. Wood Sci.*, 2012; **58(3)**: 273–278. DOI 10.1007/s10086-011-1243-5.

[10] Berardi U. and Iannace G., *Appl. Acoust.*, 2017; **115**: 131–138. DOI 10.1016/j.apacoust.2016.08.012.

[11] Chanlert P., Manoma W., Jintara A., Kerdkaew T. and Sutthibutpong T., *Chiang Mai J. Sci.*, 2023; **50(2)**: 1–17. DOI 10.12982/CMJS.2023.015.

[12] Park S.H., Lee M., Seo P.N., Kang E.C. and Kang C.W., *Bioresources*, 2020; **15(3)**: 5291–5304. DOI 10.15376/biores.15.3.5291-5304.

[13] Asasutjarit C., Hirunlabh J., Khedari J., Charoenvai S., Zeghmati B. and Shin U.C., *Constr. Build. Mater.*, 2007; **21(2)**: 277–288. DOI 10.1016/j.conbuildmat.2005.08.028.

[14] Carman P.G., *Chem. Eng. Res. Des.*, 1997; **75**: S32–S48. DOI 10.1016/s0263-8762(97)80003-2.

[15] Garai M. and Pompoli F., *Appl. Acoust.,* 2005; **66(12)**: 1383–1398. DOI 10.1016/j.apacoust.2005.04.008.

[16] Luu H.T., Perrot C., Monchiet V. and Panneton R., *J. Acoust. Soc. Am.*, 2017; **141(6)**: 4768–4780. DOI 10.1121/1.4989373.

[17] Ellison J., Koedam N.E., Wang Y., Primavera J., Eong J., Yong W.-H., et al., Nypa fruticans - The IUCN Red List of Threatened Species 2010, 2010. DOI 10.2305/IUCN.UK.2010-2.RLTS.T178800A7610085.en.

[18] Rozainah M.Z. and Aslezaeim N., *Sci.Res. Essays*, 2010; **5(24)**: 3896–3902.

[19] Cheablam O. and Chanklap B., *Scientifica (Cairo)*, 2020; **2020**: 1-20. DOI 10.1155/2020/3856203.

[20] Yub Harun N., Ameen Hezam Saeed A. and Ramachandran V.A.A., *Mater. Today Proc.*, 2021; **42**: 436–443. DOI 10.1016/j.matpr.2020.10.169.

[21] Nurdin H., Hasanuddin W. and Saddikin M., *J. Phys. Conf. Ser.*, 2019; **1387(1)**: 012103. DOI 10.1088/1742-6596/1387/1/012103.

[22] Podkumnerd N., Wunsri S. and Rattanankit T., *J. Commun. Dev. Life Qual.*, 2019; **7(3)**: 271-282.

[23] Tamunaidu P. and Saka S., *Ind. Crop. Prod.*, 2011; **34(3)**: 1423–1428. DOI 10.1016/j.indcrop.2011.04.020.

[24] Hasan A., Rabbi M.S., Billah M.M. and Hasib M.A., *Heliyon*, 2022; **8(12)**: e11967. DOI 10.1016/j.heliyon.2022.e11967.

[25] Allard J.F. and Champoux Y., *J. Acoust. Soc. Am.*, 1992; **91(6)**: 3346–3353. DOI 10.1121/1.402824.

[26] Champoux Y. and Stinson M.R., *J. Acoust. Soc. Am.*, 1992; **92(2)**: 1120–1131. DOI 10.1121/1.405281.

[27] Johnson D.L., Koplik J. and Dashen R., *J. Fluid Mech.*, 1987; **176(1)**: 379. DOI 10.1017/S0022112087000727.

[28] Lafarge D., Lemarinier P., Allard J.F. and Tarnow V., *J. Acoust. Soc. Am.*, 1997; **102(4)**: 1995–2006. DOI 10.1121/1.419690.

[29] ISO-9053-1, Acoustics-determination of airflow resistance-Part 1: Static airflow method, International Organization for Standardization, Geneva, 2018.

[30] Chanlert P., Tongyoo S. and Rordrak C., *Appl. Acoust.,* 2022; **198:** 108984. DOI 10.1016/j.apacoust.2022.108984.

[31] Chanlert P., Jintara A. and Manoma W., *Bioresources*, 2022; **17(4)**: 5612–5621. DOI 10.15376/biores.17.4.5612-5621.

[32] ASTM-E1050, Standard test method for impedance and absorption of acoustical materials using a tube, two microphones and a digital frequency analysis system, ASTM International, Pennsylvania, 1990.

[33] ISO-10534, Determination of sound absorption coefficient and impedance in impedance tubes : Part 2: Transfer-function method, International Organization for Standardization, Geneva, 1998.

[34] ASTM-E2611, Standard Test Method for Normal Incidence Determination of Porous Material Acoustical Properties Based on the Transfer Matrix Method, ASTM International, Pennsylvania, 2019.

[35] Hasan A., Rabbi M.S., Billah M.M. and Hasib M.A., *Heliyon*, 2022; **8(12)**: e11967. DOI 10.1016/j.heliyon.2022.e11967.

[36] Alves Fidelis M.E., Pereira T.V.C., Gomes O.D.F.M., De Andrade Silva F. and Toledo Filho R.D., *J. Mater. Res. Technol.*, 2013; **2(2)**: 149–157. DOI 10.1016/j.jmrt.2013.02.003.

[37] Andreassen E., Myhre O.J., Hinrichsen E.L. and Grøstad K., *J. Appl. Polym. Sci.*, 1994; **52(10)**: 1505–1517. DOI 10.1002/app.1994.070521015.

[38] Bardot A., Brouard B. and Allard J.F., *J. Appl. Phys.*, 1996; **79(11)**: 8223–8229. DOI 10.1063/1.362462.

[39] Doutres O., Atalla N. and Osman H., *J. Acoust. Soc. Am.*, 2015; **137(6)**: 3502–3513. DOI 10.1121/1.4921027.

[40] Taban E., Tajpoor A., Faridan M., Samaei S.E. and Beheshti M.H., *Acoust. Aust.*, 2019; **47(1)**: 67–77. DOI 10.1007/s40857-019-00151-8.